

1 **The changing character of twenty-first century precipitation over the**
2 **western United States in the variable-resolution CESM**

3 Xingying Huang, * Paul A. Ullrich

4 *Department of Land, Air and Water Resources, University of California, Davis*

5 *Corresponding author address: Xingying Huang, Department of Land, Air and Water Resources,
6 University of California Davis, Davis, CA 95616.
7 E-mail: xyhuang@ucdavis.edu

ABSTRACT

8 (To be added once the main content settled down)

9 **1. Introduction**

10 There is substantial and growing interest in understanding the character of precipitation within
11 a changing climate, in large part because of the pronounced impacts of water availability on
12 socioeconomic and natural systems (Hegerl et al. 2004; Kharin et al. 2007; Scoccimarro et al.
13 2013). Among these studies, precipitation extremes have been a major focus, particularly drought
14 and flood events (Seneviratne et al. 2012). Studies examining the character of precipitation in a
15 warming world, which utilize models of varying complexity from simple thermodynamic models
16 through complex coupled climate simulations, suggest that although atmospheric water vapor is
17 increasing, the consequences for precipitation are far more complicated. Extreme precipitation
18 events are particularly nuanced: Our best projections suggest that extreme precipitation events
19 will intensify even in regions where mean precipitation decreases (Tebaldi et al. 2006; Kharin
20 et al. 2007).

21 Although future climate projections are subject to large uncertainties, climate models are
22 nonetheless one of the most versatile tools for studying climate variability and extremes events
23 in the future (Easterling et al. 2000). Global climate models (GCMs) have often been used to
24 investigate changes in the mean, variability and extremes of climate, as forced with predicted
25 greenhouse gas (GHGs) concentrations and aerosol emissions (Meehl et al. 2006). Several past
26 studies have investigated global impacts (Seneviratne et al. 2012), but studies addressing impacts
27 at local and regional scales are less common. Although increased GHG concentrations have con-
28 tributed to the observed intensification of heavy precipitation events over the tropical ocean (Allan
29 and Soden 2008) and the majority of Northern Hemisphere overland areas Min et al. (2011), these
30 impacts are much more poorly understood at regional scales due to variability at finer spatial scales
31 associated with the atmospheric circulation (Trenberth 2011). As a consequence of this variability,

³² a confident assessment of changes in regional extremes requires both high spatial resolution and a
³³ long integration period.

³⁴ Insufficient regional-scale climate information has been a major outstanding problem in climate
³⁵ science, as stakeholders and water managers typically require fine-scale information on climate
³⁶ impacts in order to effectively develop adaptation and mitigation strategies. In order to reach the
³⁷ scales needed for effective local planning, dynamical downscaling with regional climate models
³⁸ (RCMs) has been typically used to ascertain the frequency, intensity, and duration of extreme
³⁹ events. By only simulating a limited regional domain, RCMs better capture fine-scale dynami-
⁴⁰ cal features under high horizontal resolution (Bell et al. 2004; Frei et al. 2006; Rauscher et al.
⁴¹ 2010; Wehner 2013). Higher resolution can also enable more accurate simulation of precipitation
⁴² extremes, which can be driven by land use, land/water contrast, snow cover, cloudiness and circu-
⁴³ lation patterns associated with topography (Leung et al. 2003a; Diffenbaugh et al. 2005; Salathé Jr
⁴⁴ et al. 2008; Wehner et al. 2010). Diffenbaugh et al. (2005) studied both heat events and wet events
⁴⁵ over the contiguous United States based on RCMs simulation at 25 km horizontal resolution, and
⁴⁶ demonstrated that fine-scale processes were critical for accurate assessment of local- and regional-
⁴⁷ scale climate change vulnerability. Leung et al. (2003b) showed that the higher-resolution RCMs
⁴⁸ yield more realistic precipitation patterns and produce more frequent heavy precipitation over the
⁴⁹ western U.S. (WUS), consistent with observations.

⁵⁰ Despite their success, RCMs also have known issues associated with inconsistency between the
⁵¹ lateral forcing data and the driven RCM, and the menu of physical parameterizations and param-
⁵² eters typically available to RCMs can lead to over-tuning of the model for a particular geographic
⁵³ region or climatological field (McDonald 2003; Laprise et al. 2008; Mesinger and Veljovic 2013).
⁵⁴ Consequently, there has been growing interest in variable-resolution enabled GCMs (VRGCMs)
⁵⁵ to improve regional climate simulations. Unlike RCMs, which require GCM data to drive the sim-

ulation at lateral boundaries, VRGCMs use a unified model with coarse global resolution and enhanced resolution over a specific study region (Staniforth and Mitchell 1978; Fox-Rabinovitz et al. 1997). VRGCMs have demonstrated comparable utility for regional climate studies at a reduced computational cost, particular when compared to uniform-resolution GCMs (Fox-Rabinovitz et al. 2006; Rauscher et al. 2013).

In this paper, we utilize the recently developed variable-resolution option in the Community Earth System Model (VR-CESM). VR-CESM is based on the CESM (and its predecessor, the Community Climate System Model (CCSM)), a family of models that have been used for decades to study the global climate (Neale et al. 2010a; Hurrell et al. 2013). The overall performance of VR-CESM for modeling regional climate in the California and Nevada is detailed in Huang et al. (2016), where it was argued that VR-CESM has competitive biases in comparison to the Weather Research and Forecasting (WRF) model (a traditional RCM) and the uniform-resolution CESM, when evaluating both against high-quality observations and reanalysis. VR-CESM has been used in a number of studies to capture fine-scale atmospheric processes (Zarzycki et al. 2014, 2015; Rhoades et al. 2015). It was also shown that VR-CESM did not suffer from apparent artifacts within the coarse-fine transition region.

This study focuses on changes in the character of precipitation over the 21st Century within the WUS, as predicted from long-term ensemble runs conducted with VR-CESM with a local grid resolution of $\sim 0.25^\circ$. The WUS is known to be particularly vulnerable to hydrological extreme events, particularly floods and droughts (Leung et al. 2003b; Caldwell 2010), and hosts a variety of local features and microclimates associated with its rough and varied topography. Simulations of the future climate are performed in accordance with the representative concentration pathway (RCP) 8.5 scenario, which describes a “business-as-usual” projection for GHGs (Riahi et al. 2011). RCP8.5 is a baseline scenario with updated base year calibration (to 2005) and no

80 explicit climate policy. In this study we focus on a single RCP since end-of-century projections
81 with the substantially more optimistic RCP2.6 scenario have been found to be qualitatively sim-
82 ilar to mid-century RCP8.5 results (which are assessed in this study). Simulations are further
83 conducted in accordance with the Atmospheric Model Intercomparison Project (AMIP) protocol
84 (Gates 1992), a widely-used approach for climate model diagnosis, validation and intercompari-
85 son that imposes global sea surface temperatures (SSTs) and sea ice. By constraining atmospheric
86 boundary conditions at the sea surface, we avoid model biases that are known to exist in the fully
87 coupled configuration (Grodsky et al. 2012; Small et al. 2014) and accept potential uncertainties
88 associated with our choice of SSTs.

89 Changes in the character of precipitation, in terms of frequency and intensity, have been assessed
90 in our study from recent history through the end of 21st century. A comprehensive set of metrics
91 for precipitation extremes have been evaluated from ensemble simulations over the 26-year peri-
92 ods corresponding to historical (1980-2005), mid-century (2025-2050) and end-of-century (2075-
93 2100). We hypothesize that spatial inhomogeneity in local geography and temperature will also
94 result in similarly inhomogeneous impacts on the precipitation field. We expect that teleconnec-
95 tions (specifically the El Niño-Southern Oscillation, ENSO) will have a pronounced impact on
96 precipitation features over particular area under the changes of mean SST and its variations. Since
97 only one SST dataset was used for this study, we note that our projections are conditioned on a
98 particular future character of ENSO. This is a potentially large source of uncertainty, as at present
99 there is no clear consensus on how ENSO may behave under a warming climate (Fedorov and
100 Philander 2000; Guilyardi et al. 2009), and strengthening or weakening of this pattern will have
101 clear consequences for our results.

102 This work builds on a number of previous studies that have explored the projected future change
103 in WUS precipitation. For example, Kim (2005) applied downscaled climate change signals to se-

104 lected indicators, and concluded that global warming induced by increased CO₂ is likely to drive
105 increases in extreme hydrologic events in the WUS. Duffy et al. (2006) found that mean precip-
106 itation predicted by the RCMs are not statistically significant compared to interannual variability
107 in many regions over WUS, although there is little consistency among the different RCMs as to
108 responses in precipitation to increased GHGs. Gao et al. (2015) pointed out a potentially large
109 increase in atmospheric river events by the end of the 21st century under the RCP8.5 scenario.

110 This paper is structured as follows. Section 2 describes the model setup. Section 3 describes
111 the methodology and reference datasets employed. An assessment of the ability of the model to
112 capture the climatology of the WUS is given in section 4. Results from the future mean climato-
113 logical trend and projected changes to precipitation indices are in section 6. Section 7 summarizes
114 the main points of the study along with further discussion.

115 2. Model Setup

116 CESM is a state-of-the-art Earth modeling framework, consisting of coupled atmosphere, ocean,
117 land and sea ice models (Neale et al. 2010b; Hurrell et al. 2013). In this study, the Community At-
118 mosphere Model version 5 (CAM5) (Neale et al. 2010b) and the Community Land Model version
119 4.0 (Oleson et al. 2010) are used. CAM5 is configured with the Spectral Element (SE) dynamical
120 core, which supports desirable conservation, accuracy and parallel scalability properties (Dennis
121 et al. 2011; Taylor 2011) and incorporates the variable-resolution option (Zarzycki et al. 2014).
122 CLM is employed in the *unigrid* configuration, which allows the land model and atmospheric
123 model to utilize the same model grid so eliminates the need for interpolation. SSTs and sea ice,
124 which are used to compute ocean-atmosphere fluxes, are prescribed in accordance with the AMIP
125 protocol (Gates 1992). The variable-resolution mesh used for this study is depicted in Figure 1, in
126 accord with our past studies (Rhoades et al. 2015; Huang et al. 2016; Huang and Ullrich 2016).

127 Simulations have been performed for the historical period (1979-2005, hereafter referred to as
128 `hist`) and for two future periods: 2024-2050 (hereafter referred to as `mid`) and 2074-2100 (hereafter
129 referred to as `end`). Daily output are recorded for each period on the native SE grid and then
130 remapped to a regional latitude-longitude mesh (??). For purposes of analysis, the first year of
131 each time period was discarded as a spin-up period to allow adequate time for the initialized land
132 and atmosphere to equilibrate. The 26-year duration was chosen to provide an adequate sampling
133 of annual variability for each time phase. As mentioned earlier, GHG concentrations are set based
134 on RCP8.5. Historical SSTs and sea ice are prescribed at 1° resolution, as described by Hurrell
135 et al. (2008). SSTs and sea ice for each future period are developed from fully-coupled RCP 8.5
136 climate simulations with bias correction applied (Cecile Hannay, personal communication). Using
137 prescribed SSTs in place of a coupled ocean model considerably reduces the computation cost and
138 so allows the atmospheric model to be run at a higher overall resolution. Annually-updated land
139 surface datasets, which prescribe land-use characteristics, are interpolated from 0.5° to the land
140 model grid.

141 Ensemble runs are needed to ensure that the sample adequately accounts for climate variability,
142 especially for statistics associated with climatological extremes. However, the exact number of
143 ensemble members required is heavily dependent on the variability of the particular metric being
144 examined, and so no standard ensemble criteria exists. Deser et al. (2012b) suggest that around
145 3 ensemble runs are required to detect a significant epoch difference for JJA (June-July-August)
146 surface temperatures, whereas 10 to 30 ensemble members are needed for that for DJF (Dec.-Jan.-
147 Feb.) precipitation. In our study, the use of prescribed SSTs does reduce the intrinsic variability
148 of the climate system (see supplement), and so we found reasonably converged results with two
149 ensemble members for the historical period and four ensemble members for each future period.

150 **3. Methodology**

151 *a. Precipitation indices*

152 Standard indices have been employed to characterize precipitation (Tebaldi et al. 2006; Zhang
153 et al. 2011; Sillmann et al. 2013). In order to choose a comprehensive (but minimal) set that are
154 informative to stakeholders and water managers, indices from throughout the literature have been
155 assessed. The indices examined include those defined by the Expert Team on Climate Change De-
156 tection and Indices (ETCCDI) (Karl et al. 1999) that are featured in earlier studies (Dulière et al.
157 2011; Sillmann et al. 2013; Diffenbaugh et al. 2005; Singh et al. 2013) and others such as return
158 levels, dry spell and wet spell characteristics defined by either percentiles or by selected thresh-
159 olds. The indices we have chosen for this study attempt to provide a relatively comprehensive
160 characterization of precipitation, and are summarized in Table 1.

161 [Paul: You should probably state at some point why you don't employ drought or dry spell
162 indices]

163 *b. Impacts of ENSO*

164 The impact of ENSO on precipitation is emphasized in our study due to its influence on precipi-
165 tation over a majority of our study area, particularly the southwest U.S. (Cayan et al. 1999; Zhang
166 et al. 2010; Deser et al. 2012a; Yoon et al. 2015). The phase of ENSO (*i.e.* El Niño and La Niña)
167 is identified each year using the Oceanic Niño Index (ONI), defined as the 3-month running means
168 of SST anomalies in the Niño 3.4 region (covering 5N-5S, 120-170W based on NOAA (2013)).
169 An El Niño or La Niña episode is said to occur when the ONI exceeds +0.5 or -0.5 for at least five
170 consecutive months for a water year (*i.e.* from July to June) (NOAA 2013) (see the supplement).
171 In order to adjust for the trend in the SST field associated with climate change, the anomaly is

172 computed against the detrended mean SSTs from the periods 1971-2000, 2020-2050 and 2070-
173 2100 for hist, mid and end respectively, using the aforementioned observed and predicted SST
174 datasets. As argued by Kao and Yu (2009), it may be desirable to use an extended Niño 3.4 region
175 to determine the phase of ENSO – however, when employing SST anomalies integrated over the
176 region 105-170W, we observed no significant impact on ONI statistics.

177 *c. Assessing statistical significance*

178 Student's t-test has been used to test whether or not two datasets at each grid point are statisti-
179 cally equivalent, if the sample population can be adequately described by a normal distribution.
180 The normality of a dataset is assessed under the Anderson-Darling test. When the sample popu-
181 lations do not approximately follow a normal distribution, Mann-Whitney-Wilcoxon (MWW) test
182 is employed in lieu of the t-test. All these tests are evaluated at the 0.05 (α) significance level.
183 When comparing different time periods, statistical tests are conducted using all years from each
184 ensemble run.

185 (add description of the supplement like what are included; see the sst_enso.pdf, mask the land
186 (over land, it should the surface temperature.))

187 *d. Reference datasets*

188 Gridded observational datasets and reanalysis of the highest available quality, with comparable
189 horizontal resolutions to our VR-CESM simulations, are used for assessing the simulation qual-
190 ity. Multiple reference datasets are necessary due to the underlying uncertainty in interpolating
191 precipitation fields. The three datasets employed are as follows:

192 **UW Gridded Data:** The 0.125° UW daily gridded meteorological data is obtained from
193 the Surface Water Modeling group at the University of Washington, covering the period

194 1949-2010 (Maurer et al. 2002; Hamlet and Lettenmaier 2005). The UW dataset imposes
195 topographic corrections by forcing the long-term average precipitation to match that of the
196 PRISM dataset.

197 **National Centers for Environmental Prediction (NCEP) Climate Prediction Center**
198 **(CPC):** This 0.25° daily-output dataset provides gauge-based analysis of daily precipitation
199 from the CPC covering the period 1948-2006. It is a unified precipitation product that cov-
200 ers the Conterminous United States and amalgamates a number of data sources at CPC via
201 optimal interpolation objective analysis.

202 **North American Regional Reanalysis (NARR):** NARR is a ~ 32 km high-resolution reanal-
203 ysis product with 3-hourly output produced by NCEP via dynamical downscaling over North
204 America and covering the period 1979-present (Mesinger et al. 2006).

205 **4. Model Assessment**

206 Before proceeding, we assess the ability of VR-CESM to represent the character of precipitation
207 over the WUS. The indices defined in Table 1 are depicted in Figures 2 and Figure 3 for VR-
208 CESM and each of the reference datasets over the historical period (1980-2005). We assume
209 equal confidence in each of the reference datasets, and use Student's t-test (with UW, CPC and
210 NARR as the three statistical samples) to identify regions where VR-CESM deviates significantly
211 from the reference mean. Regions where differences are statistically significant are identified with
212 stippling in row (a) and (e) of each figure.

213 Compared against the reference, VR-CESM largely captures the spatial patterns of precipitation
214 and its indices. As expected, the majority of precipitation distributed along the northwest coastal

215 area and the mountainous regions of the Cascades and the Sierra Nevada. Nonetheless, several
216 apparent biases are present:

217 First, VR-CESM significantly overestimates Pr over dry regions with deviations between 0.2 mm
218 to 1.5 mm, especially over the eastern flank of the Cascades and on both sides of the Sierra Nevada
219 (with relative differences reaching 50%-150%). As with many regional models, VR-CESM is
220 “dreary” and exhibits too many precipitation days ($R1mm$, $Pr \geq 1$ mm/day and $R5mm$, 1 mm/day \leq
221 $Pr \leq 5$ mm/day) [citation needed]. Nonetheless, over most regions the relative contribution of each
222 precipitation frequency subset to total precipitation ($F1mm$, $F5mm$, $F10mm$, $F20mm$, $F40mm$) is
223 fairly accurate, suggesting that the probability density function describing precipitation intensity
224 is accurately represented almost everywhere.

225 Second, the spatial pattern of precipitation variability agrees well between VR-CESM and ref-
226 erences with agreement everywhere except in the Great Plains (the eastern edge of our domain)
227 and in California’s Central Valley. The Great Plains is not a focus of this study, but the suppressed
228 variance is dominant during the warm season (April-September) and so likely represents a failure
229 of the convection scheme to adequately simulate variability in this region. This bias is also ob-
230 served in 0.25° uniform-resolution CESM simulations [citation needed to ASD data], and so is not
231 a symptom of the eastern edge of the variable-resolution transition region.

232 However, the grossly exaggerated variability over the western flank of the Sierra Nevada through
233 California’s Central Valley does merit some additional discussion. Here, the overestimation of
234 precipitation and enhanced variability is associated with too many extreme precipitation events
235 ($Pr > 20$ mm/day). This bias is related to exaggerated orographic uplift (upslope winds, not shown)
236 and is associated with a dry bias along the eastern flank of the Sierras. Similar biases in simulating
237 extreme precipitation over the topographically complex regions including the Cascades and Sierra
238 Nevada ranges have also been found in high-resolution RCM simulations Walker and Diffenbaugh

239 (2009); Singh et al. (2013), and have been primarily attributed to excessively strong winds. This
240 issue may be further impacted by the diagnostic treatment of precipitation in CAM5 [citation to
241 Morrison Gettleman 1 microphysics].

242 The representation of precipitation in VR-CESM over California was also discussed in Huang
243 et al. (2016), where it was observed that VR-CESM simulations at 0.25° adequately represented
244 regional climatological patterns with high spatial correlation. VR-CESM demonstrated compa-
245 rable performance to WRF at 27 km (which was forced with ERA-Interim reanalysis), but still
246 overestimated overall winter precipitation (by about 25%-35%) compared to reference datasets,
247 with the largest differences over the western edge of the Sierra Nevada. This bias is not allevi-
248 ated by simply increasing the spatial resolution, as experimental VR-CESM simulations at 14km,
249 7km and 3.5km show only modest improvement (Alan M. Rhoades, personal communication).
250 This suggests that the bias might be related with more complex dynamic processes rather than
251 treatment of the orographic effects.

252 CESM at 1° resolution was also assessed in order to better understand the impacts of resolution.
253 We find that precipitation patterns over complex topography are poorly represented and do not
254 capture the spatial patterns induced by orographic effects. Over the Cascades and Sierra Nevada,
255 total precipitation grossly underestimated by 1° CESM, when compared to VR-CESM, gridded
256 and reanalysis datasets (see the supplement [Point to exact figure]). Precipitation has otherwise
257 been smoothed out over the coastal areas and the mountainous regions of the northwest U.S when
258 simulated with CESM at coarse resolution. This result clearly underscores the benefits of high
259 resolution (particularly the representation of topography) in simulating precipitation features. Re-
260 sults are also provided in the supplement for the output from a globally-uniform CESM run at
261 0.25° spatial resolution with the finite volume (FV) dynamical core (Wehner et al. 2014), which
262 exhibits similar performance to VR-CESM (see the supplement [Point to exact figure]). Overall,

263 0.25° resolution appears to provide the best tradeoff between accuracy and computational cost, as
264 coarser resolution does not correctly represent precipitation features and higher resolution does
265 not appear to substantially improve model accuracy.

266 We have also assessed the impact of the ENSO signal within the historical VR-CESM runs by
267 differencing the precipitation fields between the warm phase (i.e. El Niño) and cool phase (i.e.
268 La Niña), compared to references (see the supplement). ENSO exhibits a weaker signal for obser-
269 vational precipitation, compared to VR-CESM, which might suggest that the model exaggerates
270 ENSO's impact on precipitation, especially over the northwest U.S. The improvement of ENSO
271 in the model is directly proportional to the representation of ENSO forced precipitation anomalies
272 (AchutaRao and Sperber 2006).

273 5. Drivers of climatological precipitation change

274 The remainder of this paper now focuses on model predictions of change over the 21st cen-
275 tury. Precipitation has been observed and modeled to be modified in character at both global and
276 regional scales under climate change. The observed intensification of heavy precipitation events
277 over the latter half of the twentieth century for the majority of Northern Hemisphere land areas
278 is primarily attributed to increases in GHGs (Min et al. 2011), although no significant changes in
279 the total precipitation have been observed globally (Donat et al. 2016). With the coupled impacts
280 of continued increasing CO₂ and SSTs over the coming century, precipitation will be modified by
281 both radiative changes in the lower troposphere and intensified water vapor evaporation over the
282 ocean (Allen and Ingram 2002; Sugi and Yoshimura 2004). In particular, precipitation extremes
283 are projected to intensify continuously through the end of 21st century in both dry and wet regions,
284 although these changes will be spatially heterogeneous (Donat et al. 2016).

285 In accordance with the Clausius-Clapeyron (C-C) relationship, saturation vapor pressure in the
286 atmosphere is expected to increase by $\sim 7\%$ for each 1°C increase in temperature (Allan and So-
287 den 2008). As long as a source of water vapor is present, a corresponding increase in atmospheric
288 water vapor content is expected. Naturally, evaporation over the ocean will increase with the cli-
289 mate warming, but increases in water vapor content over land may be constrained by soil moisture
290 (Cayan et al. 2010). When specific humidity is high, heavy rain events become more probable,
291 even if total precipitation is decreasing (Trenberth 2011). This suggests that global total precipi-
292 tation is expected to increase at a slower rate than precipitation extremes (Allan and Soden 2008).
293 In accordance with previous studies (e.g. (Allan and Soden 2008; O’Gorman and Schneider 2009;
294 Min et al. 2011)), changes to extreme precipitation follow the C-C relationship more closely than
295 total precipitation amount (Trenberth et al. 2003). However, the magnitude of those changes re-
296 main uncertain, since precipitation extremes are also dependent on factors such as the vertical
297 velocity profile and temperature (O’Gorman and Schneider 2009).

298 With overland water vapor constrained by soil moisture content, changes to moderate or heavy
299 precipitation events over the WUS are mainly the result of increased large-scale vapor transport
300 from the eastern Pacific Ocean rather than directly from evaporation, typically associated with
301 atmospheric rivers (ARs) and/or orographic uplift (Trenberth et al. 2003; Neiman et al. 2008).
302 Warming may lead to enhancement of the storm track, which would increase ARs along the U.S.
303 west coast with increased air water vapor content in the future (Dettinger 2011; Gao et al. 2015).
304 In the following sections, both the mean changes of precipitation and distributions of both non-
305 extreme and extreme events are investigated as projected by the VR-CESM model under climate
306 forcing.

307 The precipitation of the WUS has strong inter-annual variability caused by large-scale atmo-
308 spheric circulation mainly associated with the ENSO (Leung et al. 2003b). As a significant

309 driver of precipitation, ENSO modulates the storm track behavior over western U.S. with a north-
310 west/southwest precipitation dipole (Gershunov and Barnett 1998), as discussed in 2. The pro-
311 jected SSTs we used here states one of the possible cases of ENSO scenarios in the future. How-
312 ever, there is still substantial uncertainty regarding how El Niño will change under global warming
313 (Fedorov and Philander 2000; Guilyardi et al. 2009), which is a source of uncertainty in our results.
314 Capotondi (2013) showed that the diversity of El Niño characteristics in CCSM4 is comparable to
315 what was found in observations, although, as found by Deser et al. (2012c), the overall magnitude
316 of ENSO in CCSM4 [Paul: was this changed at all in CESM1?] is overestimated by 30% over the
317 preindustrial time period.

318 6. Results

319 a. Mean climatology

320 The mean climatological changes in VR-CESM across time periods are depicted in Figure 4.
321 Since the character of WUS precipitation has a strong seasonal contrast, changes to mean precipi-
322 tation, near-surface temperature and near-surface relative humidity are depicted for what we refer
323 to as the cool season (October to March) and the warm season (April to September).

324 As a result of enhanced GHG concentrations, mean annual near-surface temperature (T2avg)
325 increases by about 1.5 to 2 K from hist to mid and about 4 to 6 K from mid to end. Despite the
326 large spatial variation in mean seasonal temperatures, the observed change to mean temperature is
327 fairly uniform, particularly over the ocean and in coastal regions. Away from the coast there is a
328 weak gradient in the temperature change field, with the largest increase in temperatures occurring
329 towards the northeast during the cool season and towards the north during the warm season. The

330 increase in temperature is also about 0.5K and 1.0K larger during the warm season compared to
331 the cool season for `mid` and `end`, respectively.

332 Practically, whether the increase rate of the water vapor as the temperature goes up will keep the
333 same or not will directly affect the relative humidity. As water vapor reaches saturation, conden-
334 sation triggers clouds and precipitation. To understand the increasing rate of water vapor content
335 under climate warming and whether relative humidity can be remain or not, 2m relative humidity
336 (`RH`) is plotted in Figure 4.

337 Overall, `RH` remains almost the same as `hist` over the regions where temperature does not sub-
338 stantially increase. However, in regions where temperature increase is larger than 2 K, `RH` is
339 instead observed to decrease significantly relative to historical values for about 2% and 3-6%
340 compared to `mid` and `end` respectively. In fact, trends in `RH` are spatially consistent with tem-
341 perature increase but opposite in magnitude with a spatial correlation coefficient of approximately
342 0.8. `RH` remains the same or increases over the near-coastal Pacific Ocean due to the increase of
343 `T2avg` being less over the ocean compared to over land. This suggests that continental evapora-
344 tion and oceanic water vapor transport are insufficient to compensate for the air vapor capacity
345 when temperature increases to certain level, which is consistent with Joshi et al. (2008), and has
346 been observed in results by Rowell and Jones (2006) over continental and southeastern Europe
347 and Simmons et al. (2010) over low-latitude and midlatitude land areas.

348 Based on those background changes of heat and water vapor, from `hist` to `mid`, mean precipita-
349 tion showed a 0.2-0.6 mm/day increase during cool season with a largest change over northwest
350 and less than 0.2 mm/day during warm season over the **southeast part [Paul: US Southeast not**
351 **in the domain]**. From `hist` to `end`, the increase is about 0.4-1.2 mm/day during cool season with
352 also a largest change over northwest, and no notable change is observed during warm season.
353 Nonetheless, these results are statistically significant (see Figure 5). East of the Rockies, precip-

354 itation increases through mid-century (statistically significant), but this trend appears to recede
355 towards the end of the century (although these results are not significant). There is also a decrease
356 of about 0.1mm/day in total precipitation over the western flank of the Sierra Nevadas during the
357 cool season from hist to future. This decrease (about 0.15 mm/day) is also found over the Cas-
358 cades and the western coastal area during warm season from hist to mid. However, this decrease
359 is not statistically significant. Majority of the precipitation over the cool season emerged from
360 large-scale patterns, whereas warm season precipitation was from convection processes. The pre-
361 cipitation over WUS for moderate or heavy precipitation is mainly due to the large-scale water
362 flux transport from the eastern Pacific Ocean rather than directly from evaporation, mainly in the
363 form of atmospheric rivers or orographic updraft (Trenberth et al. 2003; Neiman et al. 2008).

364 The increase of mean wet season precipitation over the northwest is mainly driven by enhanced
365 orographic precipitation due to increased integrated vapor transport (IVT). The IVT increases due
366 to higher water vapor content from increased ocean evaporation, which is affected primarily by
367 climatological forcing. Over southern California, precipitation did not show significant changes
368 since no substantial increase in IVT over Eastern Pacific Ocean near southern California coast
369 is predicted, with IVT in this region driven primarily by variations in ENSO. Since precipitation
370 over the Intermountain West during warm season is mainly results from the convection processes,
371 precipitation is directly related with the changes of the relative humidity. As shown in Figure
372 4, RH has decreased over most the study area except over where the soil moisture is relatively
373 low when going to end. Further, the changes of RH are related with the soil moisture magnitude
374 accompanying the changes of latent heat flux during warm season.

375 According to previous studies (e.g. (Allen and Ingram 2002; Allan and Soden 2008; O’Gorman
376 and Schneider 2009; Min et al. 2011)), changes in more extreme precipitation follow the C-C rela-
377 tionship more closely than total precipitation amount (Trenberth et al. 2003). [Paul:

378 redundant with previous section] In order to find out the precipitation changes in a comprehensive
379 aspect based on our fine-scale simulations, analyses of different precipitation distributions are
380 focused in the following part to account for the future changes of diverse precipitation events.

381 *b. Precipitation indices*

382 To see how precipitation changes in a comprehensive way, we have analyzed detailed precipitation
383 distributions in order to account for the future changes of different precipitation events, based
384 on our simulation results. The precipitation indices are presented in Table 1. For each index, the
385 changes of precipitation character for each period, averaged over all ensemble members are plotted
386 in Figure 5 (for the indices that quantify precipitation days) and Figure 6 (for the indices describing
387 precipitation amounts). Although mean precipitation shows a weak but overall increasing trend
388 from hist to mid and mid to end (about 10-15%), the precipitation indices exhibit substantially
389 more unique character.

390 When comparing hist to mid, the total rainy days and frequency of non-extreme precipitation
391 have significantly increased (about 10-15%) mainly over the central-east and southeast part of
392 WUS, which is less obvious between mid and end. On the contrary, the frequency of non-extreme
393 precipitation have decreased significantly over the northwest region and the eastern part of the
394 Montana, Wyoming and Oregon from mid to end (about 10%). These changes are the primary
395 driver for the observed change to mean precipitation exhibited in Figure 4.

396 As for extreme precipitation frequency (i.e. days with daily Pr between 10 mm and 40 mm), the
397 number of days increases from hist to mid, but the pattern is scattered over northwest and central
398 WUS. When comparing mid to end, there is a clear and significant increase in extreme precip-
399 itation events over the northwest coastal area (about 20-30%) and eastern flank of the Cascades
400 (larger than 40%). This result is consistent with Dominguez et al. (2012), who observe a robust

401 increase in winter precipitation extremes toward the latter half of the 21st century by an ensemble
402 of RCMs. There is a slight, but insignificant decrease over the Cascades and the Sierra Nevada
403 (significance is low due to the high variability of precipitation). No notable predicted changes have
404 been observed over California.

405 [Paul: For each region it would be extremely valuable to include changes to the return frequency
406 of the most extreme events – i.e. in the Northwest a five-year storm becomes a two-year storm]

407 The associated precipitation signal under a warmer climate is more ambiguous for California
408 (Neelin et al. 2013) considering the extreme variability on interannual time scales (Dettinger
409 2011). Kim (2005) found that under global warming, heavy precipitation events show largest
410 increases in the mountainous regions of the northern California Coastal Range and the Sierra
411 Nevada. However, our results show a minor decrease (though not statistically significant) of ex-
412 treme precipitation over the Sierra Nevada. The decrease over southwest U.S. is mainly due to the
413 intensified La Niña in the future as shown in the Section 2.

414 For very extreme precipitation ($\text{Pr} \geq 40 \text{ mm}$) events, there is an increasing trend over the north-
415 west coast (larger than 60%) and the Cascades (about 50%) and its eastern flank (larger than 60%)
416 when comparing `hist` to `end`. Significant changes have also been observed over the northern moun-
417 tainous part of California for about 20-40% from `hist` to `end`. The corresponding changes in rain
418 amount are consistent with the changes of frequency (see Figure 6). Overall, these results indi-
419 cate more extreme precipitation over the northwest U.S. with changes in precipitation extremes
420 following more consistently with the C-C relationship.

421 In order to understand the drivers behind the observed changes, we first examine change in
422 moisture flux for cool seasons when WUS precipitation is primarily from water vapor influx from
423 the Pacific Ocean (see Figure 7). We observe an increase in specific humidity at 850 hPa that
424 accompanies the increase of the temperature in future. However, when comparing to `hist`, westerly

425 wind tends to weaken in mid and end over the eastern part of the WUS and strengthen over western
426 area.

427 IVT (Figure 7) for extreme precipitation days over cool seasons. Generally, IVT is useful to
428 understand extreme precipitation events that arise from atmospheric rivers over the northwestern
429 U.S. and from orographic uplift (especially for very extreme precipitation) (Ralph et al. 2004;
430 Leung and Qian 2009; Dettinger 2011). Based on the observed change in IVT, it is clear that the
431 increase in moisture influx from past to future, which is mainly due to the change of the air water
432 vapor content with increased temperature, corresponds to the changes of precipitation extremes
433 shown in Figure 5.

434 1) QUANTILE CORRELATION ANALYSIS

435 To see if changes in mean precipitation can be used to predict changes in extreme precipitation
436 features, the correlations between Pr and specific quantiles have been calculated. Here, selected
437 quantiles including the values at 70% (70p), 80% (80p), 90% (90p), 95% (95p) and 99% (99p)
438 are applied based on the all the daily precipitation data at each grid point within each time period.
439 These quantiles are chosen in order to account for the changes of both moderation and extreme
440 precipitation. The mean Pr and those quantiles for hist, and the differences of these quantities
441 among different time periods can be found in the supplemental figure. Within expectation, regions
442 with higher Pr are associated with larger values of those quantiles, i.e. stronger precipitation
443 extremes. This is further supported by the high correlation (about 0.7-0.9) between Pr and R20mm,
444 R40mm, and Rxmm, not between Pr and non-extreme precipitation events.

445 Spatial correlation is assessed by computing Pearson product-moment coefficient of linear corre-
446 lation between relevant variables. It is found that the absolute changes of Pr in future are positively
447 related with the absolute changes of the quantiles. This relationship is at a moderate level between

448 mid and hist (larger than 0.65), and becomes stronger when going to the end period (reaching
449 ~0.96). Consistently, the mean Pr itself is also positively correlated with the absolute changes of
450 the quantiles in future (around 0.5 to 0.78), except 70p between end and mid and 99p mid and
451 hist.

452 The relative changes of quantiles are also related with the relative changes of Pr with correla-
453 tions around 0.65 to 0.85, except 70p and 80p between end and mid. So, the area featured with
454 higher increase of extreme precipitations in future also tends to have larger increase of its mean
455 precipitation. However, the wetter area does not necessary have more intense changes of moder-
456 ate and extreme precipitation than drier area. The changes of Pr is not obviously correlated with
457 the changes of precipitation indices, which further states that mean precipitation and precipitation
458 events undergo different features of changing in the future.

459 For further investigation of the regional heterogeneity, the frequency distributions of daily rainy
460 days for specific four regions are depicted based on simulation outputs at each gridpoint over
461 26 years of each time period (see Figure 8). We can see over the northwest, Pr intensifies with
462 upper tail going more extreme in the future, especially during end. No notable difference can be
463 observed for California area, except with more extreme upper tail for Pr exceeding 100 mm/day
464 during end, which is due to the increased precipitation extremes over the northern California as
465 shown in Figure 6. Over the inter-mountainous region, similar trends of changes can be seen
466 as the northwest area, with intensified mean and extreme precipitation. For the southwest area,
467 precipitation tends to be more extreme with a moderate level, although no notable difference exists
468 between mid and end.

469 2) ISOLATING DIFFERENCES DUE TO CLIMATE CHANGE AND ENSO

470 The phase of ENSO is well known to have important repercussions on precipitation extremes
471 (Larkin and Harrison 2005; Allan and Soden 2008; Maloney et al. 2014; Yoon et al. 2015). Cai
472 et al. (2014) found a significantly increase for extraordinary precipitation along the eastern Pacific
473 Ocean in the 21st century within the CMIP5 ensemble, associated with increasing frequency of
474 extreme El Niño events due to greenhouse warming. In this part, we will figure out how the ENSO
475 impacts specific regions over our study area, and whether the effects pattern will change over time.

476 ENSO from past to future, the difference of precipitation behaviors between the warm phase (i.e.
477 El Niño) and cool phase (i.e. La Niña) of ENSO is illustrated in Figure 9 for the wet seasons of
478 each time period. Based on the ONI index values, the mean SST anomalies are 1.38, 1.71 and 2.30
479 K during El Niño years, and -1.16, -1.62 and -1.43 K during La Niña years for hist, mid and end
480 respectively. The mean SSTs over the Niño 3.4 region where the are 26.83, 28.62 and 30.54°C
481 for textsfhist, mid and end respectively. Based on the SST datasets we used here, the anomaly
482 of ENSO has intensified. The SST anomalies of each year and each month, and their associated
483 spatial pattern when averaged during the warm and cool phases can be found in the supplement,
484 exhibiting the increasing frequency of El Niño during for mid and almost doubled frequency of La
485 Niña during mid and end compared to the hist.

486 (Huang: As SSTs increase in the future, is not it normal for the anomaly of ENSO to be increased
487 to compensate the changes of water vapor capacity? Might email Neale about this.)

488 During the El Niño phase, intensified mean precipitation is expected over the southwest (Ham-
489 let and Lettenmaier 2007), along with reduced precipitation intensity over the northwest. In La
490 Niña phase, the pattern is essentially reversed, with wetter conditions in the northwest and a drier
491 situation in the Southwest. This feature is characterized as a northwest/southwest precipitation

492 dipole, triggered by ENSO's modification of the storm track (Gershunov and Barnett 1998; Le-
493 ung et al. 2003b), along with modulation of the enhanced precipitation variability (Cayan et al.
494 1999; Kahya and Dracup 1994). This dipole is also apparently in the frequency of rainy days and
495 extreme precipitation events.

496 In mid and hist, ENSO is observed to intensify, which appears to be related with the changes
497 of the strength of El Niño and La Niña. This can be explained by the SST anomaly magnitude
498 (detrended) of warm and cold phases (see the supplement). DeFlorio et al. (2013) also found a
499 statistically significant linkages with ENSO and PDO for both the overall and extreme intensity
500 of wintertime precipitation over the WUS using CCSM4 (earlier form of CESM). Strengthening
501 storm patterns associated with ENSO are also found by Maloney et al. (2014) over California using
502 CMIP5 output under RCP8.5.

503 We have also checked the teleconnection effect of Pacific Decadal Oscillation (PDO) and it
504 did not show strong effect alone. Precipitation features did not change notably when at the cool
505 phase or warm phase of PDO during hist. However, together with ENSO at the same phase,
506 PDO can have notable effect over northwest. This coupled effect has been found by previous
507 studies Gershunov and Barnett (1998), stating ENSO and PDO can "reinforce" each other with
508 PDO responding to the same internal atmospheric variability as ENSO (Pierce 2002). **In our**
509 **simulations, the patterns of PDO phases differs quite a bit from past to future, though there were**
510 **roughly an equal number of positive PDO years and negative PDO years in the data. We suppose**
511 **that our 26 years simulation time period might not be long enough to account for the variability of**
512 **PDO due to its duration for decades. Therefore, in this study, the PDO is not specifically analyzed.**

513 The impact of ENSO is further observed by the IVT difference over rainy days between El Niño
514 and La Niña (see Figure 10) accompanying by the wind pattern difference at 850 hPa, showing the

515 increase of the moisture flux for the southwest and decrease for the northwest. This suggests the
516 major role of moisture influx regulation of ENSO.

517 Based on the above results, it can be seen that the magnitude of the effects of ENSO is compara-
518 ble or even higher than the impacts of climate forcing. For further investigation, linear regression
519 is applied to signaling the factor effects due to ENSO and climate forcing. First, we get the SST
520 anomaly of each cool season when ENSO mainly affect followed by the way of Niño 3.4 to be
521 the ENSO factor values. Then, we use the GHGs values at each year to represent the climate
522 forcing factor. The features of the precipitation indices as we defined above are used as response
523 variables. Combined the values of all the time period and all the runs, we got the significance of
524 these two factors' effects at each grid point based on the ANOVA (analysis of variance) output
525 (see the supplement). Changing of the SSTs anomaly can affect most of the study area for non-
526 extreme precipitation events, and southern regions and the Cascades and the Rocky Mountains for
527 precipitation extremes. The GHGs factor mainly shows significant impacts over the northwest and
528 inter-mountainous regions for both non-extreme and extreme precipitation events.

529 We have also examined the linear coefficients of these two factors over where their effects are
530 significant to see the strength that ENSO and GHGs play at each grid point (see the supplement). It
531 is found that the effect of the ENSO is similar to the pattern of the difference between El Niño and
532 La Niña (see Figure 10). In contrast, the effect of the GHGs is close to the pattern of the difference
533 between the different time periods (see Figure 5). We do acknowledge that the values might not be
534 accurate due to the simple linear mode we used here. However, the qualitative conclusions won't
535 change. Therefore, we assume that even the ENSO largely regulates the precipitation over different
536 phases, it won't affect our results shown here for the changes of precipitation features from past to
537 future. Although here is just one of the possible cases of ENSO scenarios in the future, as ENSO

538 behavior is strongly dependent on choice of climate models, the underlying principles should still
539 be consistent.

540 Although, the strength of ENSO intensifies in the future with CESM, there is still substantial
541 uncertainty regarding how El Niño will change under global warming as debated by plenty of
542 studies (Fedorov and Philander 2000; Guilyardi et al. 2009), particularly as ENSO appears to be
543 relatively insensitive to a doubling of CO₂ in most models (DiNezio et al. 2012). Correctly simula-
544 tion changes to the spatial pattern of SSTs ion state-of-the-art coupled GCMs remains challenging
545 Joseph and Nigam (2006); ?); Jha et al. (2014); Taschetto et al. (2014).

546 7. Discussion and Summary

547 The increased cool season precipitation extremes tend to result in higher runoff events over
548 the northwest U.S., which are in turn associated with a greater chance of flooding and a loss of
549 snowpack. A decrease in counts of rainy days during the warm season over central and southern
550 California, though small in magnitude, will probably intensify the drought condition due to the
551 deficit of soil moisture with higher evapotranspiration caused by the warmer climate in the future
552 Cayan et al. (2010); Bell et al. (2004).

553 (Huang: Yoon et al. (2015) found a strengthened relation with ENSO for the projected increase
554 in water cycle extremes in California using the output from CESM1 and CMIP5. Similarly by
555 Maloney et al. (2014) using CMIP5 dataset. (check the CESM1?))

556 (Summary is to be added once the main content have been settled down The contribution of
557 human-induced increases in greenhouse gases to the character of precipitation is confounded by
558 patterns of variability in the atmospheric circulation. Consistent with previous studies, changes
559 in more extreme precipitation follow the Clausius-Clapeyron relationship more closely than total
560 precipitation amount. The changes of the strength of ENSO remains uncertain. However, the char-

561 actor of ENSO appears to be the largest factor in understanding changing precipitation extremes
562 in the U.S. West.)

563 *Acknowledgments.* The authors would like to thank Michael Wehner for sharing the dataset and
564 many suggestions. The authors also want to thank Alan M. Rhoades for providing the simulation
565 output. We acknowledge the substantial efforts behind the datasets used in this study, including
566 UW, NCDC and NARR. The simulation data used is available by request at xyhuang@ucdavis.edu.
567 This project is supported in part by the xxx and by the xxx.

568 References

- 569 AchutaRao, K., and K. R. Sperber, 2006: Enso simulation in coupled ocean-atmosphere models:
570 are the current models better? *Climate Dynamics*, **27** (1), 1–15.
- 571 Allan, R. P., and B. J. Soden, 2008: Atmospheric warming and the amplification of precipitation
572 extremes. *Science*, **321** (5895), 1481–1484.
- 573 Allen, M. R., and W. J. Ingram, 2002: Constraints on future changes in climate and the hydrologic
574 cycle. *Nature*, **419** (6903), 224–232.
- 575 Bell, J. L., L. C. Sloan, and M. A. Snyder, 2004: Regional changes in extreme climatic events: a
576 future climate scenario. *Journal of Climate*, **17** (1), 81–87.
- 577 Cai, W., and Coauthors, 2014: Increasing frequency of extreme el niño events due to greenhouse
578 warming. *Nature climate change*, **4** (2), 111–116.
- 579 Caldwell, P., 2010: California wintertime precipitation bias in regional and global climate models.
580 *Journal of Applied Meteorology and Climatology*, **49** (10), 2147–2158.

- 581 Capotondi, A., 2013: Enso diversity in the ncar ccsm4 climate model. *Journal of Geophysical*
582 *Research: Oceans*, **118 (10)**, 4755–4770.
- 583 Cayan, D. R., T. Das, D. W. Pierce, T. P. Barnett, M. Tyree, and A. Gershunov, 2010: Future
584 dryness in the southwest us and the hydrology of the early 21st century drought. *Proceedings of*
585 *the National Academy of Sciences*, **107 (50)**, 21 271–21 276.
- 586 Cayan, D. R., K. T. Redmond, and L. G. Riddle, 1999: ENSO and hydrologic extremes in the
587 western United States*. *Journal of Climate*, **12 (9)**, 2881–2893.
- 588 DeFlorio, M. J., D. W. Pierce, D. R. Cayan, and A. J. Miller, 2013: Western us extreme precipita-
589 tion events and their relation to enso and pdo in ccsm4. *Journal of Climate*, **26 (12)**, 4231–4243.
- 590 Dennis, J., and Coauthors, 2011: CAM-SE: A scalable spectral element dynamical core for the
591 Community Atmosphere Model. *International Journal of High Performance Computing Appli-*
592 *cations*, 1094342011428142.
- 593 Deser, C., R. Knutti, S. Solomon, and A. S. Phillips, 2012a: Communication of the role of natural
594 variability in future north american climate. *Nature Climate Change*, **2 (11)**, 775–779.
- 595 Deser, C., A. Phillips, V. Bourdette, and H. Teng, 2012b: Uncertainty in climate change projec-
596 tions: the role of internal variability. *Climate Dynamics*, **38 (3-4)**, 527–546.
- 597 Deser, C., and Coauthors, 2012c: Enso and pacific decadal variability in the community climate
598 system model version 4. *Journal of Climate*, **25 (8)**, 2622–2651.
- 599 Dettinger, M., 2011: Climate change, atmospheric rivers, and floods in california—a multimodel
600 analysis of storm frequency and magnitude changes1. Wiley Online Library.

- 601 Diffenbaugh, N. S., J. S. Pal, R. J. Trapp, and F. Giorgi, 2005: Fine-scale processes regulate the
602 response of extreme events to global climate change. *Proceedings of the National Academy of*
603 *Sciences of the United States of America*, **102** (44), 15 774–15 778.
- 604 DiNezio, P. N., B. P. Kirtman, A. C. Clement, S.-K. Lee, G. A. Vecchi, and A. Wittenberg, 2012:
605 Mean climate controls on the simulated response of enso to increasing greenhouse gases. *Journal*
606 *of Climate*, **25** (21), 7399–7420.
- 607 Dominguez, F., E. Rivera, D. Lettenmaier, and C. Castro, 2012: Changes in winter precipitation
608 extremes for the western united states under a warmer climate as simulated by regional climate
609 models. *Geophysical Research Letters*, **39** (5).
- 610 Donat, M. G., A. L. Lowry, L. V. Alexander, P. A. OGorman, and N. Maher, 2016: More extreme
611 precipitation in the world [rsquor] s dry and wet regions. *Nature Climate Change*.
- 612 Duffy, P., and Coauthors, 2006: Simulations of present and future climates in the western United
613 States with four nested regional climate models. *Journal of Climate*, **19** (6), 873–895.
- 614 Duli re, V., Y. Zhang, and E. P. Salath  Jr, 2011: Extreme Precipitation and Temperature over the
615 US Pacific Northwest: A Comparison between Observations, Reanalysis Data, and Regional
616 Models*. *Journal of Climate*, **24** (7), 1950–1964.
- 617 Easterling, D. R., G. A. Meehl, C. Parmesan, S. A. Changnon, T. R. Karl, and L. O. Mearns, 2000:
618 Climate extremes: observations, modeling, and impacts. *science*, **289** (5487), 2068–2074.
- 619 Fedorov, A. V., and S. G. Philander, 2000: Is el ni o changing? *Science*, **288** (5473), 1997–2002.
- 620 Fox-Rabinovitz, M., J. C te, B. Dugas, M. D qu , and J. L. McGregor, 2006: Variable resolution
621 general circulation models: Stretched-grid model intercomparison project (SGMIP). *Journal of*
622 *Geophysical Research: Atmospheres (1984–2012)*, **111** (D16).

- 623 Fox-Rabinovitz, M. S., G. L. Stenchikov, M. J. Suarez, and L. L. Takacs, 1997: A finite-
624 difference GCM dynamical core with a variable-resolution stretched grid. *Monthly weather*
625 **review**, **125** (11), 2943–2968.
- 626 Frei, C., R. Schöll, S. Fukutome, J. Schmidli, and P. L. Vidale, 2006: Future change of precipita-
627 tion extremes in Europe: Intercomparison of scenarios from regional climate models. *Journal*
628 *of Geophysical Research: Atmospheres (1984–2012)*, **111** (D6).
- 629 Gao, Y., J. Lu, L. R. Leung, Q. Yang, S. Hagos, and Y. Qian, 2015: Dynamical and thermodynami-
630 cal modulations on future changes of landfalling atmospheric rivers over western north america.
631 *Geophysical Research Letters*, **42** (17), 7179–7186.
- 632 Gates, W. L., 1992: AMIP: The Atmospheric Model Intercomparison Project. *Bulletin of the*
633 *American Meteorological Society*, **73**, 1962–1970.
- 634 Gershunov, A., and T. P. Barnett, 1998: Interdecadal modulation of enso teleconnections. *Bulletin*
635 *of the American Meteorological Society*, **79** (12), 2715–2725.
- 636 Grodsky, S. A., J. A. Carton, S. Nigam, and Y. M. Okumura, 2012: Tropical atlantic biases in
637 ccesm4. *Journal of Climate*, **25** (11), 3684–3701.
- 638 Guilyardi, E., A. Wittenberg, A. Fedorov, M. Collins, C. Wang, A. Capotondi, G. J. Van Olden-
639 borgh, and T. Stockdale, 2009: Understanding el niño in ocean-atmosphere general circulation
640 models. *Bulletin of the American Meteorological Society*, **90** (3), 325.
- 641 Hamlet, A. F., and D. P. Lettenmaier, 2005: Production of Temporally Consistent Gridded Precipi-
642 tation and Temperature Fields for the Continental United States*. *Journal of Hydrometeorology*,
643 **6** (3), 330–336.

- 644 Hamlet, A. F., and D. P. Lettenmaier, 2007: Effects of 20th century warming and climate variability
645 on flood risk in the western us. *Water Resources Research*, **43** (6).
- 646 Hegerl, G. C., F. W. Zwiers, P. A. Stott, and V. V. Kharin, 2004: Detectability of anthropogenic
647 changes in annual temperature and precipitation extremes. *Journal of Climate*, **17** (19), 3683–
648 3700.
- 649 Huang, X., A. M. Rhoades, P. A. Ullrich, and C. M. Zarzycki, 2016: An evaluation of the vari-
650 able resolution-cesm for modeling california's climate. *Journal of Advances in Modeling Earth*
651 *Systems*.
- 652 Huang, X., and P. A. Ullrich, 2016: Irrigation impacts on california's climate with the variable-
653 resolution cesm. *Journal of Advances in Modeling Earth Systems*.
- 654 Hurrell, J. W., J. J. Hack, D. Shea, J. M. Caron, and J. Rosinski, 2008: A new sea surface temper-
655 ature and sea ice boundary dataset for the Community Atmosphere Model. *Journal of Climate*,
656 **21** (19), 5145–5153.
- 657 Hurrell, J. W., and Coauthors, 2013: The community earth system model: A framework for col-
658 laborative research. *Bulletin of the American Meteorological Society*, **94** (9), 1339–1360.
- 659 Jha, B., Z.-Z. Hu, and A. Kumar, 2014: Sst and enso variability and change simulated in historical
660 experiments of cmip5 models. *Climate dynamics*, **42** (7-8), 2113–2124.
- 661 Joseph, R., and S. Nigam, 2006: Enso evolution and teleconnections in ipcc's twentieth-century
662 climate simulations: Realistic representation? *Journal of Climate*, **19** (17), 4360–4377.
- 663 Joshi, M. M., J. M. Gregory, M. J. Webb, D. M. Sexton, and T. C. Johns, 2008: Mechanisms for
664 the land/sea warming contrast exhibited by simulations of climate change. *Climate Dynamics*,
665 **30** (5), 455–465.

- 666 Kahya, E., and J. A. Dracup, 1994: The influences of type 1 el nino and la nina events on stream-
667 flows in the pacific southwest of the united states. *Journal of Climate*, **7 (6)**, 965–976.
- 668 Kao, H.-Y., and J.-Y. Yu, 2009: Contrasting eastern-pacific and central-pacific types of enso.
669 *Journal of Climate*, **22 (3)**, 615–632.
- 670 Karl, T. R., N. Nicholls, and A. Ghazi, 1999: Clivar/gcos/wmo workshop on indices and indicators
671 for climate extremes workshop summary. *Weather and Climate Extremes*, Springer, 3–7.
- 672 Kharin, V. V., F. W. Zwiers, X. Zhang, and G. C. Hegerl, 2007: Changes in temperature and
673 precipitation extremes in the IPCC ensemble of global coupled model simulations. *Journal of
674 Climate*, **20 (8)**, 1419–1444.
- 675 Kim, J., 2005: A projection of the effects of the climate change induced by increased co2 on
676 extreme hydrologic events in the western us. *Climatic Change*, **68 (1-2)**, 153–168.
- 677 Laprise, R., and Coauthors, 2008: Challenging some tenets of regional climate modelling. *Meteo-
678 rology and Atmospheric Physics*, **100 (1-4)**, 3–22.
- 679 Larkin, N. K., and D. Harrison, 2005: On the definition of el niño and associated seasonal average
680 us weather anomalies. *Geophysical Research Letters*, **32 (13)**.
- 681 Leung, L. R., L. O. Mearns, F. Giorgi, and R. L. Wilby, 2003a: Regional climate research: needs
682 and opportunities. *Bulletin of the American Meteorological Society*, **84 (1)**, 89–95.
- 683 Leung, L. R., and Y. Qian, 2009: Atmospheric rivers induced heavy precipitation and flooding in
684 the western US simulated by the WRF regional climate model. *Geophysical research letters*,
685 **36 (3)**.

- 686 Leung, L. R., Y. Qian, and X. Bian, 2003b: Hydroclimate of the western United States based on
687 observations and regional climate simulation of 1981-2000. Part I: Seasonal statistics. *Journal*
688 *of Climate*, **16 (12)**, 1892–1911.
- 689 Maloney, E. D., and Coauthors, 2014: North american climate in cmip5 experiments: part iii:
690 assessment of twenty-first-century projections*. *Journal of Climate*, **27 (6)**, 2230–2270.
- 691 Maurer, E., A. Wood, J. Adam, D. Lettenmaier, and B. Nijssen, 2002: A long-term hydrologically
692 based dataset of land surface fluxes and states for the conterminous United States*. *Journal of*
693 *climate*, **15 (22)**, 3237–3251.
- 694 McDonald, A., 2003: Transparent boundary conditions for the shallow-water equations: testing in
695 a nested environment. *Monthly weather review*, **131 (4)**, 698–705.
- 696 Meehl, G. A., H. Teng, and G. Bannister, 2006: Future changes of el niño in two global coupled
697 climate models. *Climate Dynamics*, **26 (6)**, 549–566.
- 698 Mesinger, F., and K. Veljovic, 2013: Limited area NWP and regional climate modeling: a test
699 of the relaxation vs Eta lateral boundary conditions. *Meteorology and Atmospheric Physics*,
700 **119 (1-2)**, 1–16.
- 701 Mesinger, F., and Coauthors, 2006: North American regional reanalysis. *Bulletin of the American*
702 *Meteorological Society*, **87**, 343–360.
- 703 Min, S.-K., X. Zhang, F. W. Zwiers, and G. C. Hegerl, 2011: Human contribution to more-intense
704 precipitation extremes. *Nature*, **470 (7334)**, 378–381.
- 705 Neale, R. B., and Coauthors, 2010a: Description of the NCAR community atmosphere model
706 (CAM 5.0). *NCAR Tech. Note NCAR/TN-486+ STR*.

- 707 Neale, R. B., and Coauthors, 2010b: Description of the NCAR Community Atmosphere Model
708 (CAM 5.0). NCAR Technical Note NCAR/TN-486+STR, National Center for Atmospheric Re-
709 search, Boulder, Colorado, 268 pp.
- 710 Neelin, J. D., B. Langenbrunner, J. E. Meyerson, A. Hall, and N. Berg, 2013: California winter
711 precipitation change under global warming in the coupled model intercomparison project phase
712 5 ensemble. *Journal of Climate*, **26** (17), 6238–6256.
- 713 Neiman, P. J., F. M. Ralph, G. A. Wick, J. D. Lundquist, and M. D. Dettinger, 2008: Meteorolog-
714 ical characteristics and overland precipitation impacts of atmospheric rivers affecting the west
715 coast of north america based on eight years of ssm/i satellite observations. *Journal of Hydrom-
716 eteorology*, **9** (1), 22–47.
- 717 NOAA, 2013: Defining El Niño and La Niña. Accessed: 2015-
718 08-20, [https://www.climate.gov/news-features/understanding-climate/
719 watching-el-nio-and-la-nia-noaa-adapts-global-warming](https://www.climate.gov/news-features/understanding-climate/watching-el-nio-and-la-nia-noaa-adapts-global-warming).
- 720 O’Gorman, P. A., and T. Schneider, 2009: The physical basis for increases in precipitation ex-
721 tremes in simulations of 21st-century climate change. *Proceedings of the National Academy of
722 Sciences*, **106** (35), 14 773–14 777.
- 723 Oleson, K., and Coauthors, 2010: Technical description of version 4.0 of the Community Land
724 Model (CLM). NCAR Technical Note NCAR/TN-478+STR, National Center for Atmospheric
725 Research, Boulder, Colorado, 257 pp. doi:10.5065/D6FB50WZ.
- 726 Pierce, D. W., 2002: The role of sea surface temperatures in interactions between enso and the
727 north pacific oscillation. *Journal of climate*, **15** (11), 1295–1308.

- 728 Ralph, F. M., P. J. Neiman, and G. A. Wick, 2004: Satellite and caljet aircraft observations of
729 atmospheric rivers over the eastern north pacific ocean during the winter of 1997/98. *Monthly*
730 *Weather Review*, **132** (7), 1721–1745.
- 731 Rauscher, S. A., E. Coppola, C. Piani, and F. Giorgi, 2010: Resolution effects on regional climate
732 model simulations of seasonal precipitation over Europe. *Climate dynamics*, **35** (4), 685–711.
- 733 Rauscher, S. A., T. D. Ringler, W. C. Skamarock, and A. A. Mirin, 2013: Exploring a Global
734 Multiresolution Modeling Approach Using Aquaplanet Simulations. *Journal of Climate*, **26** (8),
735 2432–2452.
- 736 Rhoades, A. M., X. Huang, P. A. Ullrich, and C. M. Zarzycki, 2015: Characterizing Sierra Nevada
737 snowpack using variable-resolution CESM. *Journal of Applied Meteorology and Climatology*,
738 **(2015)**.
- 739 Riahi, K., and Coauthors, 2011: RCP 8.5A scenario of comparatively high greenhouse gas emis-
740 sions. *Climatic Change*, **109** (1-2), 33–57.
- 741 Rowell, D. P., and R. G. Jones, 2006: Causes and uncertainty of future summer drying over europe.
742 *Climate Dynamics*, **27** (2-3), 281–299.
- 743 Salathé Jr, E. P., R. Steed, C. F. Mass, and P. H. Zahn, 2008: A High-Resolution Climate Model
744 for the US Pacific Northwest: Mesoscale Feedbacks and Local Responses to Climate Change*.
745 *Journal of Climate*, **21** (21), 5708–5726.
- 746 Scoccimarro, E., M. Zampieri, A. Bellucci, A. Navarra, and Coauthors, 2013: Heavy precipitation
747 events in a warmer climate: results from CMIP5 models. *Journal of climate*.

- 748 Seneviratne, S. I., and Coauthors, 2012: Changes in climate extremes and their impacts on the
749 natural physical environment. *Managing the risks of extreme events and disasters to advance*
750 *climate change adaptation*, 109–230.
- 751 Sillmann, J., V. Kharin, F. Zwiers, X. Zhang, and D. Bronaugh, 2013: Climate extremes indices
752 in the cmip5 multimodel ensemble: Part 2. future climate projections. *Journal of Geophysical*
753 *Research: Atmospheres*, **118 (6)**, 2473–2493.
- 754 Simmons, A., K. Willett, P. Jones, P. Thorne, and D. Dee, 2010: Low-frequency variations
755 in surface atmospheric humidity, temperature, and precipitation: Inferences from reanalyses
756 and monthly gridded observational data sets. *Journal of Geophysical Research: Atmospheres*,
757 **115 (D1)**.
- 758 Singh, D., M. Tsiang, B. Rajaratnam, and N. S. Diffenbaugh, 2013: Precipitation extremes over the
759 continental United States in a transient, high-resolution, ensemble climate model experiment.
760 *Journal of Geophysical Research: Atmospheres*, **118 (13)**, 7063–7086.
- 761 Small, R. J., and Coauthors, 2014: A new synoptic scale resolving global climate simulation using
762 the community earth system model. *Journal of Advances in Modeling Earth Systems*, **6 (4)**,
763 1065–1094.
- 764 Staniforth, A. N., and H. L. Mitchell, 1978: A variable-resolution finite-element technique for
765 regional forecasting with the primitive equations. *Monthly Weather Review*, **106 (4)**, 439–447.
- 766 Sugi, M., and J. Yoshimura, 2004: A mechanism of tropical precipitation change due to co2
767 increase. *Journal of climate*, **17 (1)**, 238–243.

- 768 Taschetto, A. S., A. S. Gupta, N. C. Jourdain, A. Santoso, C. C. Ummenhofer, and M. H. England,
769 2014: Cold tongue and warm pool enso events in cmip5: mean state and future projections.
770 *Journal of Climate*, **27 (8)**, 2861–2885.
- 771 Taylor, M. A., 2011: Conservation of mass and energy for the moist atmospheric primitive equa-
772 tions on unstructured grids. *Numerical Techniques for Global Atmospheric Models*, Springer,
773 357–380.
- 774 Tebaldi, C., K. Hayhoe, J. M. Arblaster, and G. A. Meehl, 2006: Going to the extremes. *Climatic
775 change*, **79 (3-4)**, 185–211.
- 776 Trenberth, K. E., 2011: Changes in precipitation with climate change. *Climate Research*, **47 (1)**,
777 123.
- 778 Trenberth, K. E., A. Dai, R. M. Rasmussen, and D. B. Parsons, 2003: The changing character of
779 precipitation. *Bulletin of the American Meteorological Society*, **84 (9)**, 1205–1217.
- 780 Walker, M. D., and N. S. Diffenbaugh, 2009: Evaluation of high-resolution simulations of daily-
781 scale temperature and precipitation over the united states. *Climate dynamics*, **33 (7-8)**, 1131–
782 1147.
- 783 Wehner, M. F., 2013: Very extreme seasonal precipitation in the NARCCAP ensemble: model
784 performance and projections. *Climate Dynamics*, **40 (1-2)**, 59–80.
- 785 Wehner, M. F., R. L. Smith, G. Bala, and P. Duffy, 2010: The effect of horizontal resolution
786 on simulation of very extreme US precipitation events in a global atmosphere model. *Climate
787 dynamics*, **34 (2-3)**, 241–247.

- 788 Wehner, M. F., and Coauthors, 2014: The effect of horizontal resolution on simulation qual-
789 ity in the Community Atmospheric Model, CAM5.1. *J. Model. Earth. Sys.*, doi:10.1002/
790 2013MS000276.
- 791 Yoon, J.-H., S. S. Wang, R. R. Gillies, B. Kravitz, L. Hipps, and P. J. Rasch, 2015: Increasing
792 water cycle extremes in California and in relation to ENSO cycle under global warming. *Nature*
793 *communications*, **6**.
- 794 Zarzycki, C. M., C. Jablonowski, and M. A. Taylor, 2014: Using Variable-Resolution Meshes
795 to Model Tropical Cyclones in the Community Atmosphere Model. *Monthly Weather Review*,
796 **142** (3), 1221–1239.
- 797 Zarzycki, C. M., C. Jablonowski, D. R. Thatcher, and M. A. Taylor, 2015: Effects of localized grid
798 refinement on the general circulation and climatology in the Community Atmosphere Model.
799 *Journal of Climate*, **(2015)**.
- 800 Zhang, X., L. Alexander, G. C. Hegerl, P. Jones, A. K. Tank, T. C. Peterson, B. Trewin, and
801 F. W. Zwiers, 2011: Indices for monitoring changes in extremes based on daily temperature and
802 precipitation data. *Wiley Interdisciplinary Reviews: Climate Change*, **2** (6), 851–870.
- 803 Zhang, X., J. Wang, F. W. Zwiers, and P. Y. Groisman, 2010: The influence of large-scale climate
804 variability on winter maximum daily precipitation over North America. *Journal of Climate*,
805 **23** (11), 2902–2915.
- 806 update the mesh grid plot
- 807 update the plot with new label levels

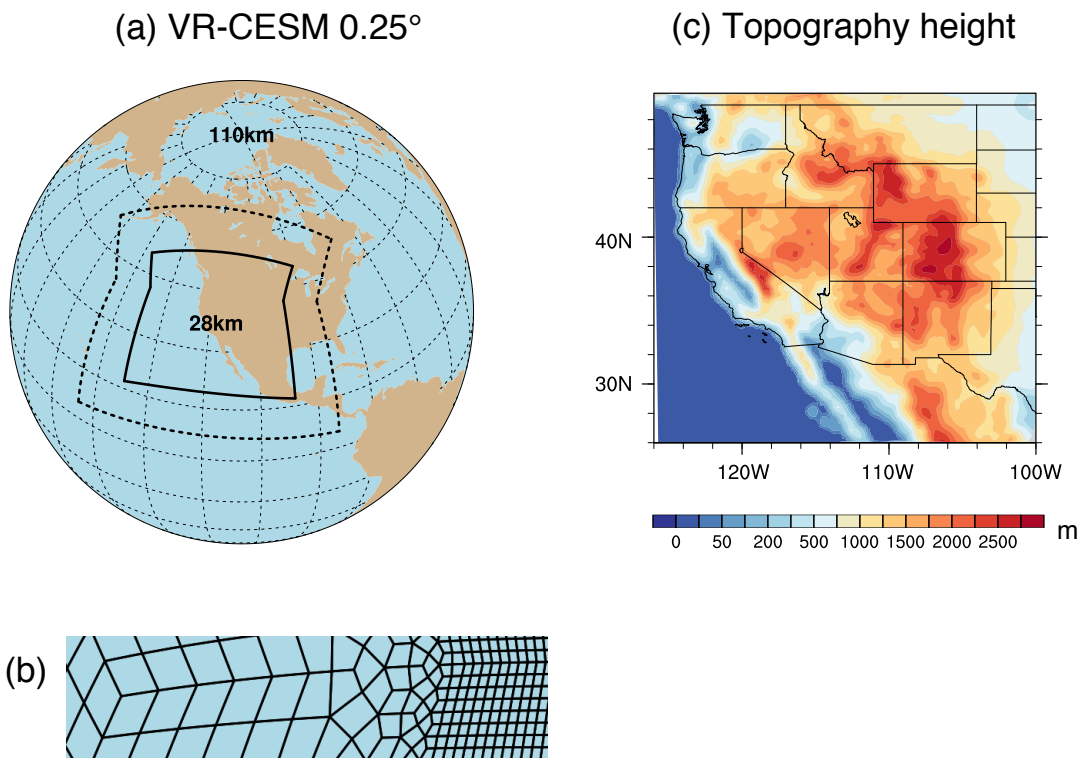
808 LIST OF TABLES

TABLE 1. Precipitation indices employed in this study.

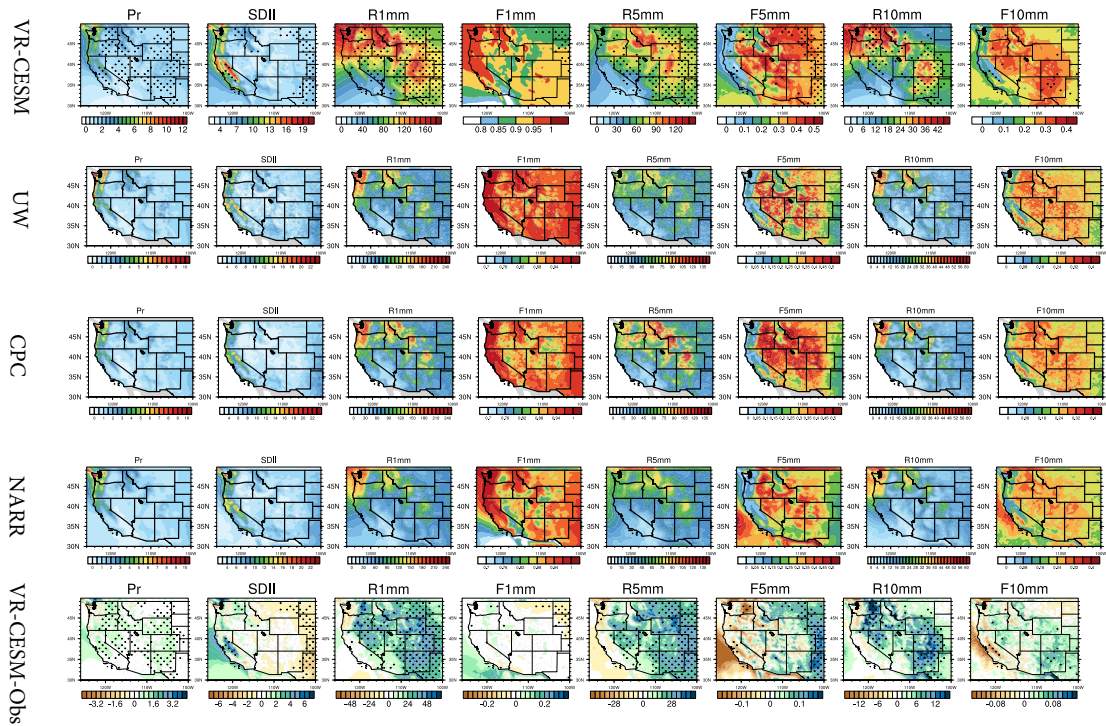
Name	Definition
Pr	Mean daily precipitation
R1mm	Number of days per year with Pr>1 mm
SDII	Simple precipitation intensity index: Precipitation amount / $\langle R1mm \rangle$ (mm/day)
R5mm	Number of days per year with Pr>1 mm and Pr=<5 mm
R10mm	Number of days per year with Pr>5 mm and Pr=<10 mm
R20mm	Number of days per year with Pr>10 mm and Pr=<20 mm
R40mm	Number of days per year with Pr>20 mm and Pr=<40 mm
Rxmm	Number of days per year with Pr>40 mm
F1mm	Fraction of precipitation contributed to the total precipitation for days of R1mm (similarly for F5mm, F10mm, F20mm, F40mm and Fxmm)
P5mm	Precipitation amount from R5mm (similarly for P10mm, P20mm, F40mm, Pxmm)

810 LIST OF FIGURES

811	Fig. 1. (a) The approximate grid spacing used for the VR-CESM 0.25° mesh. (b) A depiction of 812 the transition from the global 1° resolution mesh through two layers of refinement to 0.25° . 813 (c) Topography height over the study area.	42
814	Fig. 2. Mean precipitation and other related indices from VR-CESM and reference datasets over 815 1980-2005. (Note: Grids with statistically significance difference are marked with stip- 816 pling.)	43
817	Fig. 3. The mean precipitation and other related indices from VR-CESM and reference datasets 818 over 1980-2005 (continued).	44
819	Fig. 4. The mean precipitation (Pr), 2m average temperature ($T2avg$), and 2m relative humidity 820 (RH) averaged over each time period. (Note: Grids with statistically significance difference 821 for the RH are marked with stippling.)	45
822	Fig. 5. Differences of precipitation behaviors from past to future over WUS averaged of each time 823 period. (Note: Grids with statistically significance difference are marked with stippling.)	46
824	Fig. 6. Differences of precipitation behaviors from past to future over WUS averaged of each time 825 period (continued).	47
826	Fig. 7. Changes of specific humidity and horizontal wind pattern at 850hPa for moisture flux il- 827 lustration, and IVT for simulations under different time period of wet season (October to 828 March). (Note: The minimum wind vector is set to be 0.5 m/s, therefore, the wind less than 829 0.5 m/s is also plotted at the minimum length for better visualization.) For all difference 830 plots, make sure to use a common [min,max] range as its currently difficult to tease out dif- 831 ferences. Difference plots should also use a different color table to the mean results (perhaps 832 a single color color table?).	48
833	Fig. 8. Frequency distribution of rainy days ($Pr >= 0.1\text{mm/day}$) over the three time periods from 834 simulations in four regions (with logarithmic vertical scale). (Note: Region 1 to 4 cover 835 Washington and Oregon; California; Nevada, Utah and Idaho; Arizona and New Mexico, 836 respectively.)	49
837	Fig. 9. Difference of precipitation behaviors between warm and cool phases of ENSO from past to 838 future over WUS averaged of each time period.	50
839	Fig. 10. Changes of IVT for simulations under different phases of ENSO of wet season (October to 840 March). (Note: The minimum wind vector is set to be 0.5 m/s, therefore, the wind less than 841 0.5 m/s is also plotted at the minimum length for better visualization.)	51

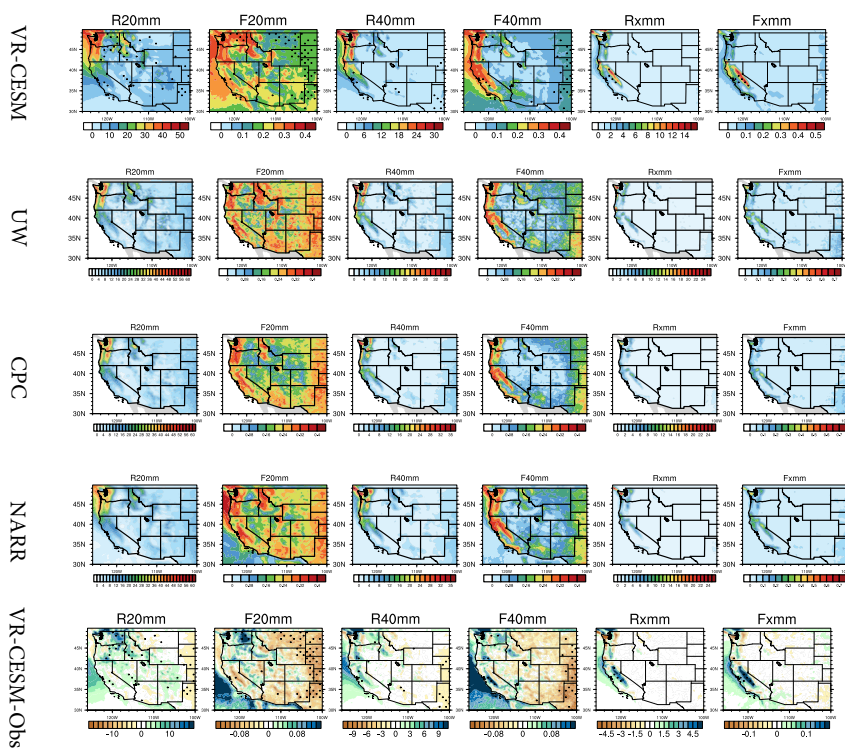


842 FIG. 1. (a) The approximate grid spacing used for the VR-CESM 0.25° mesh. (b) A depiction of the transition
 843 from the global 1° resolution mesh through two layers of refinement to 0.25° . (c) Topography height over the
 844 study area.

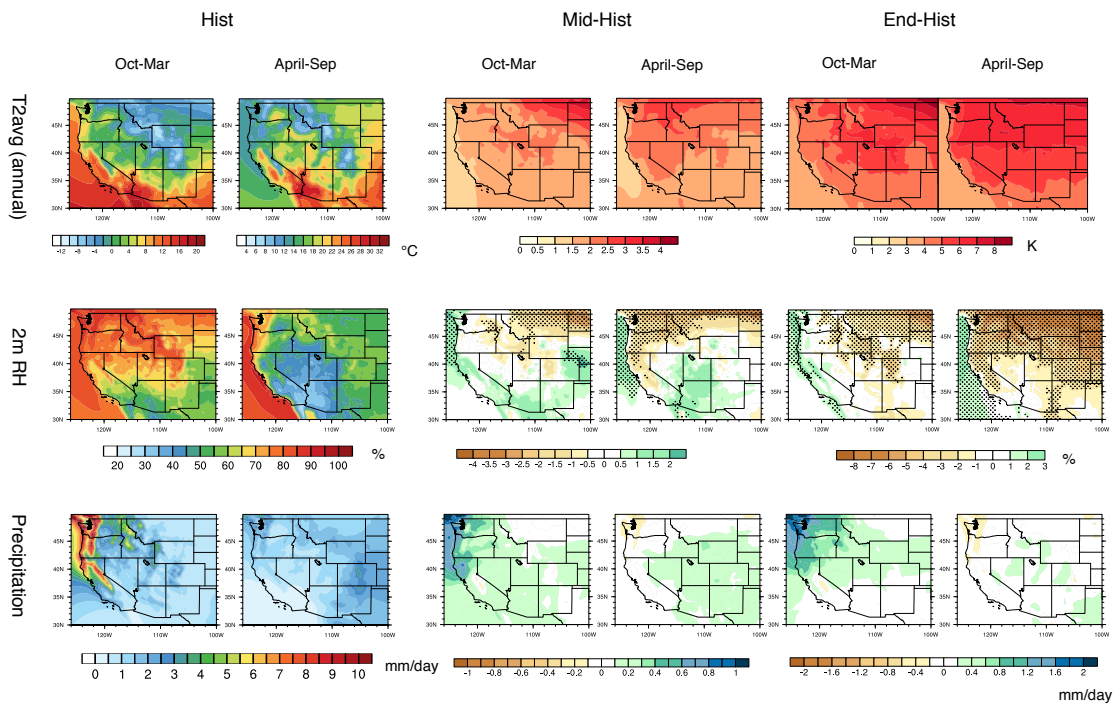


845 FIG. 2. Mean precipitation and other related indices from VR-CESM and reference datasets over 1980-2005.

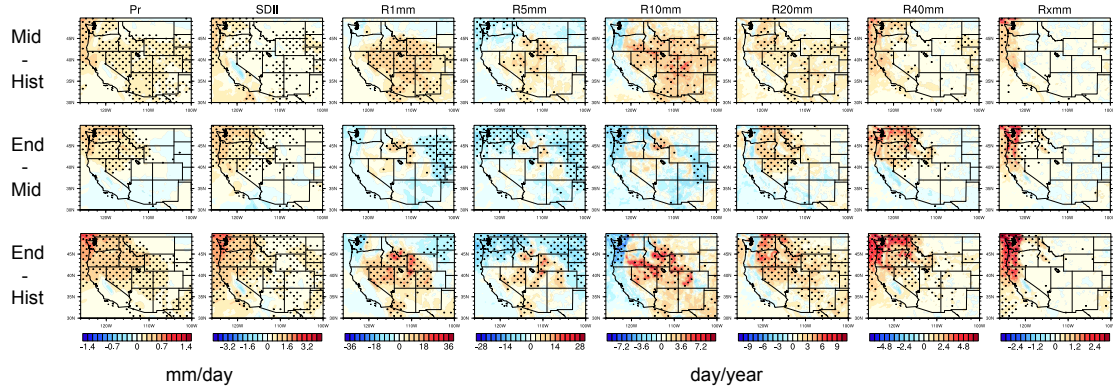
846 (Note: Grids with statistically significance difference are marked with stippling.)



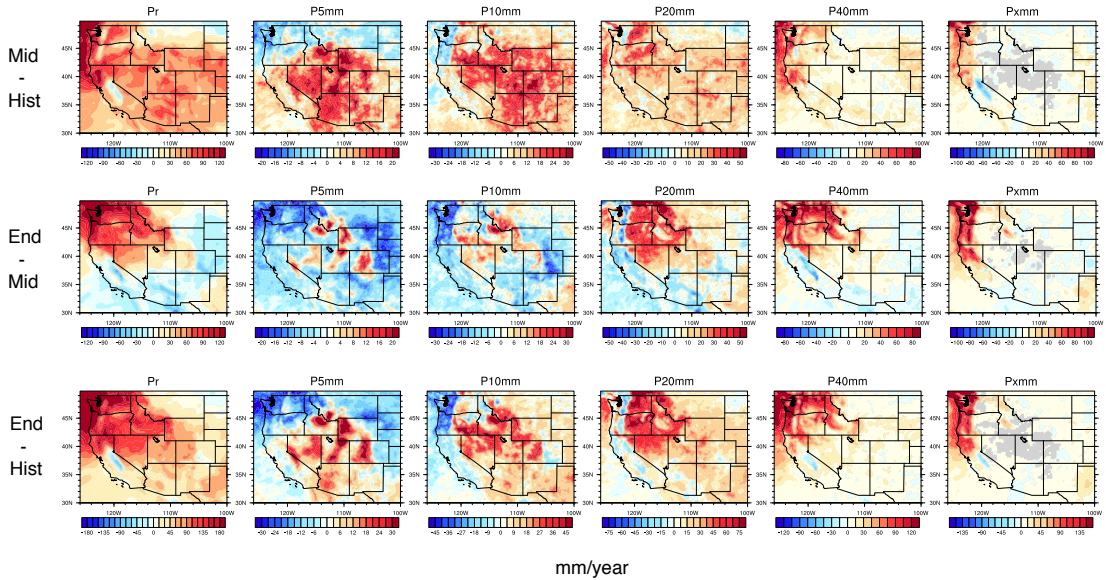
847 FIG. 3. The mean precipitation and other related indices from VR-CESM and reference datasets over 1980-
 848 2005 (continued).



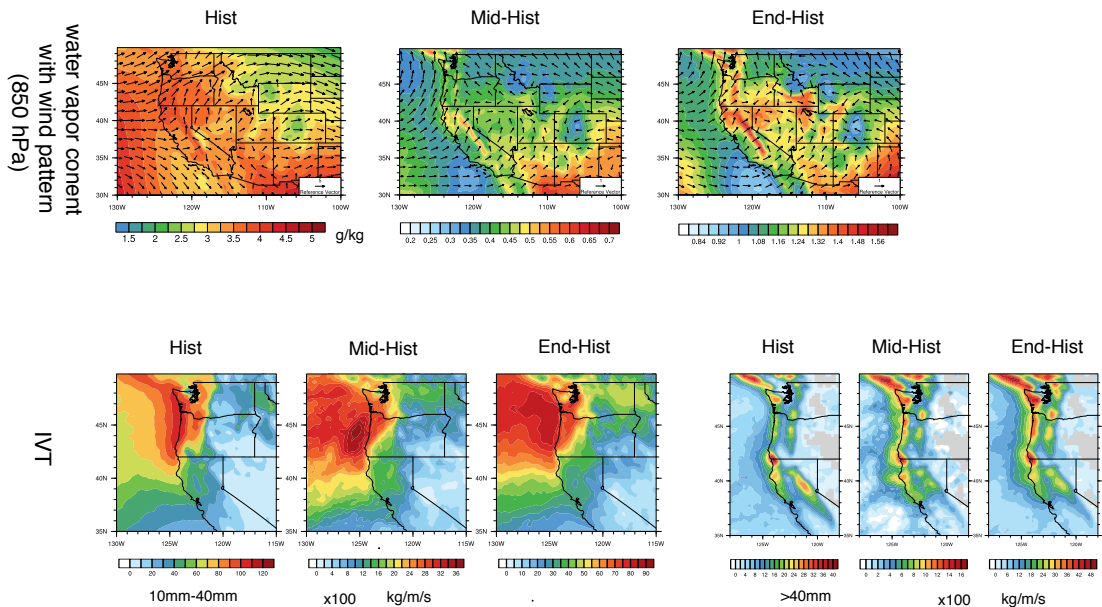
849 FIG. 4. The mean precipitation (Pr), 2m average temperature (T2avg), and 2m relative humidity (RH) aver-
 850 aged over each time period. (Note: Grids with statistically significance difference for the RH are marked with
 851 stippling.)



852 FIG. 5. Differences of precipitation behaviors from past to future over WUS averaged of each time period.
 853 (Note: Grids with statistically significance difference are marked with stippling.)



854 FIG. 6. Differences of precipitation behaviors from past to future over WUS averaged of each time period
 855 (continued).



856 FIG. 7. Changes of specific humidity and horizontal wind pattern at 850hPa for moisture flux illustration, and
 857 IVT for simulations under different time period of wet season (October to March). (Note: The minimum wind
 858 vector is set to be 0.5 m/s, therefore, the wind less than 0.5 m/s is also plotted at the minimum length for better
 859 visualization.) For all difference plots, make sure to use a common [min,max] range as its currently difficult
 860 to tease out differences. Difference plots should also use a different color table to the mean results (perhaps a
 861 single color color table?).

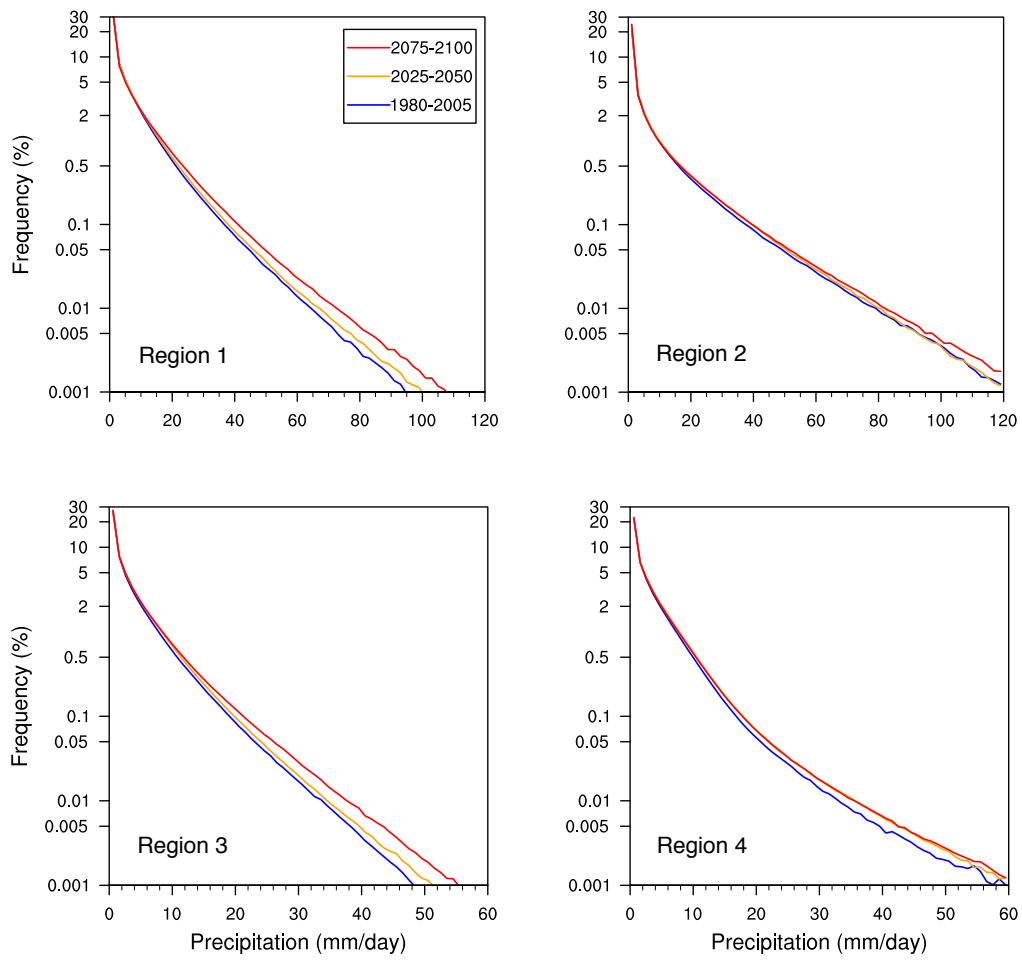
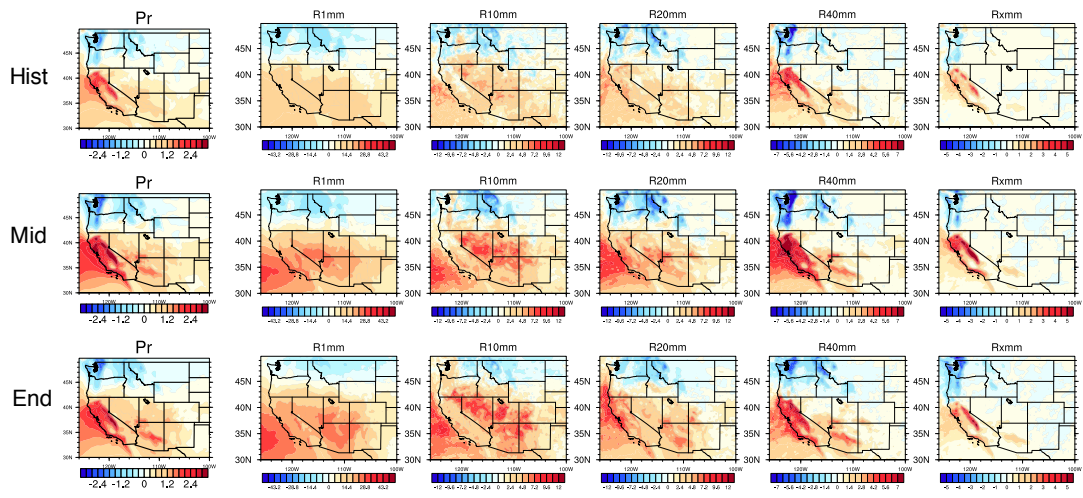
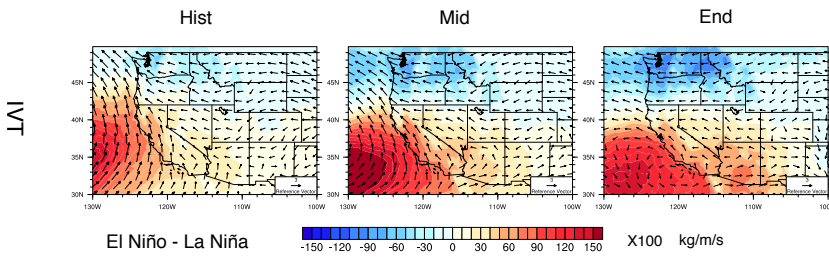


FIG. 8. Frequency distribution of rainy days ($Pr \geq 0.1 \text{ mm/day}$) over the three time periods from simulations in four regions (with logarithmic vertical scale). (Note: Region 1 to 4 cover Washington and Oregon; California; Nevada, Utah and Idaho; Arizona and New Mexico, respectively.)



865 FIG. 9. Difference of precipitation behaviors between warm and cool phases of ENSO from past to future
866 over WUS averaged of each time period.



867 FIG. 10. Changes of IVT for simulations under different phases of ENSO of wet season (October to March).
 868 (Note: The minimum wind vector is set to be 0.5 m/s, therefore, the wind less than 0.5 m/s is also plotted at the
 869 minimum length for better visualization.)